On-board Integrated Battery Chargers for Electric Vehicles Using Nine-Phase Machines

Ivan Subotic, *Student Member, IEEE*, Emil Levi, *Fellow, IEEE*, Martin Jones, and Dušan Graovac, *Senior Member, IEEE*

***Abstract* – The paper considers on-board battery charging of electrical vehicles (EV) using a three-phase voltage source and a nine-phase propulsion motor. The nine-phase inverter and induction machine are fully integrated into the charging process. The proposed integrated on-board battery charger has an advantage of unity power factor operation with no torque production in the machine during the charging mode. Moreover, there is no need for any hardware reconfiguration between the charging and propulsion mode. The principle of the charging mode operation is based on the additional degrees of freedom that exist in nine-phase machines and that can be conveniently utilized to achieve charging through the machine's stator windings with zero electromagnetic torque. Detailed theoretical analysis is reported for asymmetrical and symmetrical nine-phase systems. For both systems control in the charging mode is discussed, and the theoretical considerations are validated by simulations.**

***Index Terms*— Battery chargers, electric vehicles, multiphase machines.**

I. Introduction

DUE to fossil fuel shortage and the global warming-related problems, internal combustion engine (ICE) vehicles will be replaced in the near future at a faster rate with EVs. Some countries have already adopted action plans for this transition. In the US the forecast is for one million EVs by 2015 [1], while in the Netherlands the same number is anticipated until 2025 [2]. In order to accomplish this changeover, some of the main goals that need to be achieved are an increase in the battery capacity, and development of suitable, preferably on-board, battery chargers, capable of realising fast battery charging that complies with grid standards [3, 4].

Battery chargers can be classified into two categories: off-board and on-board, and both types come in many configurations [5]. Yet, only on-board chargers allow the user a freedom of charging from almost any single-phase or three-phase (as appropriate) power socket. Also, on-board chargers in combination with EVs' batteries are seen as a possible solution for the mass energy storage problem, which is currently one of the main concerns in the electric energy sector. EVs are for most of the time parked; hence, if integrated into the smart grid, they can accumulate the energy from the grid when the demand for the energy is low, and supply the grid with the energy when the demand is high (vehicle-to-grid, i.e. V2G concept) [6, 7]. This requires a bidirectional on-board battery charger. It can be concluded that even in a futuristic scenario where off-board charging stations might be widely available, on-board chargers will still be very desirable.

On the other hand, commonly employed on-board battery chargers have, in addition to mentioned advantages, also a few shortcomings. Nowadays, the most of them are made like a separate unit, which increases the cost of the vehicle by introducing new power-electronics elements. Depending on the model, these additional costs can be up to $ 3,000 [8]. Installation of separate charging unit requires additional space and increases the weight. However, all these shortcomings can be overcome by integrating the existing powertrain components, mainly propulsion motor and power electronics, into the charging process [9]. An integrated charger was introduced for the first time in 1985 [10], and many integrated solutions have been reported since [11].

Presently, a majority of EVs employ either induction or permanent magnet synchronous machines for propulsion [12], which are typically with three-phase stator winding. Nevertheless, at the moment only four integrated on-board solutions [13-16] allow fast (three-phase) charging incorporating these types of machines. Yet, only the solution of [16] has an advantage of no torque development in the machine during the charging. It uses mid-points of each of the three windings of a three-phase machine to attach them to a three-phase ac grid during charging. Hence the machine operates as a three-phase one in propulsion mode, while it is an equivalent of a symmetrical six-phase machine in the charging mode; the half-windings of each phase in spatial opposition are paralleled for the charging and are thus supplied with the same currents, causing cancellation of the rotating field. The solution is currently being considered for use in future EVs by Valeo [17]. Moreover, it currently presents the only on-board integrated fast (three-phase) charging configuration in general without the requirement of hardware reconfiguration between the charging and propulsion mode of operation. This paper attempts to provide two new charging solutions with the same advantages, incorporating asymmetrical and symmetrical nine-phase machines into the charging process.

Multiphase drives are primarily considered for high

The authors would like to acknowledge the Engineering and Physical Sciences Research Council (EPSRC) for supporting the Vehicle Electrical Systems Integration (VESI) project (EP/I038543/1).

I. Subotic, E. Levi and M. Jones are with the Liverpool John Moores University, School of Engineering, Technology and Maritime Operations, Liverpool L3 3AF, U.K. (+44-151 231 2257; e.levi@ljmu.ac.uk).

D. Graovac is with Infineon Technologies AG, Am Campeon 1-12, D-85579 Neubiberg, Germany.

power/high current applications. Their advantages over three-phase systems are related to the reduced power rating of the semiconductor switches and superb fault-tolerant operation capabilities [18, 19]. Nine-phase machines are characterised with existence of additional degrees of freedom with regard to the control. This yields an added benefit over their three-phase counterparts in applications related to the integrated on-board charging of EVs, as will be shown in this paper. These additional degrees of freedom can be utilised for integrated charging of a battery without any torque production in the machine.

As noted, this paper presents two novel multiphase integrated on-board chargers with unity power factor capability and the machine kept naturally at standstill during the charging process. The inverter and the machine are fully integrated into the charging process. Stator winding's leakage inductances are utilised for filtering.

The paper is organized as follows. In Section II, detailed theoretical analysis is reported for a symmetrical nine-phase integrated charging system. The same is done for an asymmetrical nine-phase system in Section III. Section IV describes the control algorithm for the proposed configurations in the charging mode of operation. Finally, in Section V theoretical results are validated by simulations. The conclusions are given in Section VI.

II. Analysis of a Symmetrical Nine-phase Charging System

Nine-phase machines with three sets of three-phase windings and three isolated neutral points are particularly suitable for vehicular applications due to their ability of being integrated into the three-phase charging process. If grid connections are attached to the neutral points of the machine, then charging without any hardware reconfiguration and with no average torque developed is possible. Non-existence of the average torque in the machine during the charging process is achieved by simultaneous identical switch control of all inverter legs belonging to the same set.

Charging without hardware reconnections demands three isolated neutral points. Hence, given the phase number $n = ak$, the number of sub-windings needs to be $a = 3$. The number of phases of the sub-windings can be $k = 3, 5, \ldots$ Since in the charging mode there will be k phases connected in parallel, this means that the equivalent leakage inductance available for the charging process will reduce more and more as the number of sub-winding phases k increases. It is for this reason that only the configurations with $k = 3$ and $a = 3$ are discussed further on. This in essence comes down to asymmetrical and symmetrical nine-phase machines with three isolated neutral points in the propulsion mode.

If a symmetrical nine-phase machine is considered first, the starting point is the nine-phase case of the general multiphase decoupling transformation matrix for multiphase systems, given in power invariant form in [19]. The matrix can be written in terms of 2D space vectors as (symbol f stands for current or voltage; indices α, β denote the flux/torque producing plane, and indices x, y stand for non-flux/torque producing planes):

$$\begin{aligned}
\underline{f}_{\alpha\beta} &= \sqrt{2/9}(f_a + \underline{a} f_b + \underline{a}^2 f_c + \underline{a}^3 f_d + \underline{a}^4 f_e + \\
&\quad + \underline{a}^5 f_f + \underline{a}^6 f_g + \underline{a}^7 f_h + \underline{a}^8 f_i) \\
\underline{f}_{x1y1} &= \sqrt{2/9}(f_a + \underline{a}^2 f_b + \underline{a}^4 f_c + \underline{a}^6 f_d + \underline{a}^8 f_e + \\
&\quad + a^{10} f_f + \underline{a}^{12} f_g + \underline{a}^{14} f_h + \underline{a}^{16} f_i) \\
\underline{f}_{x2y2} &= \sqrt{2/9}(f_a + \underline{a}^3 f_b + \underline{a}^6 f_c + \underline{a}^9 f_d + \underline{a}^{12} f_e + \\
&\quad + \underline{a}^{15} f_f + \underline{a}^{18} f_g + \underline{a}^{21} f_h + \underline{a}^{24} f_i) \\
\underline{f}_{x3y3} &= \sqrt{2/9}(f_a + \underline{a}^4 f_b + \underline{a}^8 f_c + \underline{a}^{12} f_d + \underline{a}^{16} f_e + \\
&\quad + \underline{a}^{20} f_f + \underline{a}^{24} f_g + \underline{a}^{28} f_h + \underline{a}^{32} f_i) \\
f_0 &= \sqrt{1/9}(f_a + f_b + f_c + f_d + f_e + f_f + f_g + f_h + f_i)
\end{aligned} \tag{1}$$

where $\underline{a} = \exp(j\alpha) = \cos\alpha + j\sin\alpha$ and $\alpha = 2\pi/9$. The grid currents are given with:

$$i_{kg} = \sqrt{2} I \cos(\omega t - l 2\pi/3) \qquad l = 0,1,2 \qquad k = a,b,c \tag{2}$$

The proposed connection diagram for charging mode is shown in Fig. 1. It can be seen that no hardware reconfiguration is required to change from propulsion to charging mode, which is a great advantage of the solution. The correlation between machine phase currents and grid currents is given with

$$i_a = i_d = i_g = i_{ag}/3 \qquad i_b = i_e = i_h = i_{bg}/3 \qquad i_c = i_f = i_i = i_{cg}/3 \tag{3}$$

Substitution of (2) and (3) into (1) leads to the following space vectors of the four planes of the nine-phase machine:

$$\begin{aligned}
\underline{i}_{\alpha\beta} &= 0 & \underline{i}_{x1y1} &= 0 \\
\underline{i}_{x2y2} &= I\exp(j\omega t) & \underline{i}_{x3y3} &= 0
\end{aligned} \tag{4}$$

The zero-sequence component is equal to zero. As is obvious from (4), the charging process, which is obtained without hardware reconfiguration, will utilise only the x_2-y_2 plane, and the α-β plane will stay without excitation; hence there will be no average torque developed and the rotor will not move. The only requirement is that the machine is with near-sinusoidal flux (magneto-motive force) distribution.

III. Analysis of an Asymmetrical Nine-phase System

The same charging principle can be applied to an asymmetrical nine-phase machine. The charging scheme remains to be as in Fig. 1. The general decoupling matrix [19] can no longer be used. However, it can be shown that the decoupling matrix in space vector form is, for the machine with a single neutral point, given with [20]

$$\begin{aligned}
\underline{f}_{\alpha\beta} &= \sqrt{2/9}(f_a + \underline{a} f_b + \underline{a}^2 f_c + \underline{a}^6 f_d + \\
&\quad + \underline{a}^7 f_e + \underline{a}^8 f_f + \underline{a}^{12} f_g + \underline{a}^{13} f_h + \underline{a}^{14} f_i)
\end{aligned} \tag{5a}$$

$$\begin{aligned}
\underline{f}_{x1y1} &= \sqrt{2/9}(f_a + \underline{a}^3 f_b + \underline{a}^6 f_c + \underline{a}^0 f_d + \\
&\quad + \underline{a}^3 f_e + \underline{a}^6 f_f + \underline{a}^0 f_g + \underline{a}^3 f_h + \underline{a}^6 f_i)
\end{aligned} \tag{5b}$$

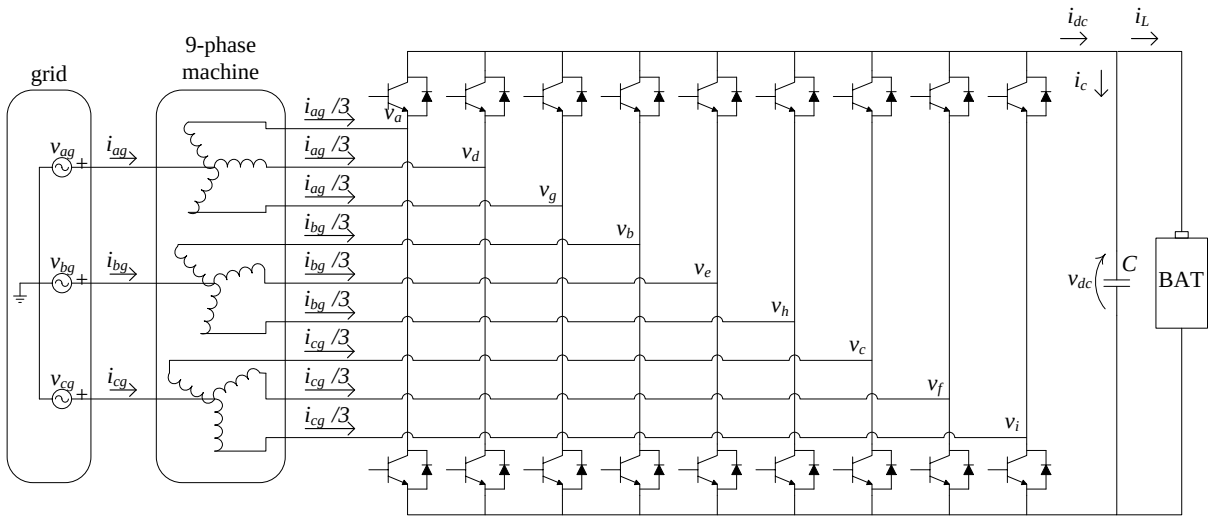

Fig. 1. Topology of the nine-phase fast integrated on-board battery charger. Triple three-phase stator winding of the machine can be in symmetrical or asymmetrical configuration.

$$\underline{f}_{x2y2} = \sqrt{2/9}(f_a + \underline{a}^5 f_b + \underline{a}^{10} f_c + \underline{a}^{12} f_d + \\ + \underline{a}^{17} f_e + \underline{a}^4 f_f + \underline{a}^6 f_g + \underline{a}^{11} f_h + \underline{a}^{16} f_i) \quad (5c)$$

$$\underline{f}_{x3y3} = \sqrt{2/9}(f_a + \underline{a}^7 f_b + \underline{a}^{14} f_c + \underline{a}^6 f_d + \\ + \underline{a}^{13} f_e + \underline{a}^2 f_f + \underline{a}^{12} f_g + \underline{a} f_h + \underline{a}^8 f_i) \quad (5d)$$

where $\underline{a} = \exp(j\alpha) = \cos\alpha + j\sin\alpha$ and $\alpha = \pi/9$. The grid currents and the correlation between machine phase currents and grid currents are again given with (2) and (3), respectively. The zero-sequence component is now governed with [20]:

$$f_0 = \sqrt{1/9}\left(f_a - f_b + f_c + f_d - f_e + f_f + f_g - f_h + f_i\right) \quad (6)$$

Substitution of (2) and (3) into (5) gives the following space vectors:

$$\underline{i}_{\alpha\beta} = 0 \qquad \underline{i}_{x2y2} = 0 \qquad \underline{i}_{x3y3} = 0$$
$$\underline{i}_{x1y1} = I\{(2/3)\cos(\omega t) + (1/\sqrt{3})\sin(\omega t) - j(1/\sqrt{3})\cos(\omega t)\} \quad (7)$$

while the zero-sequence component has the value of:

$$i_0 = -(\sqrt{8}/3) I \cos(\omega t - 2\pi/3) \quad (8)$$

As is obvious from (7), the charging process will once more not utilize the α-β plane.

Excitations of active planes for both configurations are presented in Fig. 2. The active plane currents in the case of asymmetrical machine are smaller in magnitude, since they are complemented with the zero-sequence current of (8) to produce the overall phase currents.

Presented theoretical derivations confirm that both symmetrical and asymmetrical nine-phase machines can be used for charging purposes without generation of the rotating field in the α-β plane. As shown in [21] nine-phase machines are particularly suited for EVs applications due to their high efficiency, wide speed range for flux weakening, and easiness of sensorless control implementation in propulsion mode of operation. Moreover, it is shown here that in the charging mode for these types of multiphase machines there is no need for any hardware reconfiguration as the grid connections can stay attached to the neutral points of each three-phase winding in the machine without interfering with the propulsion mode of operation. The solution of course requires a nine-phase machine with three isolated neutral points, but there are no requirements for contactors and intervention of any kind when

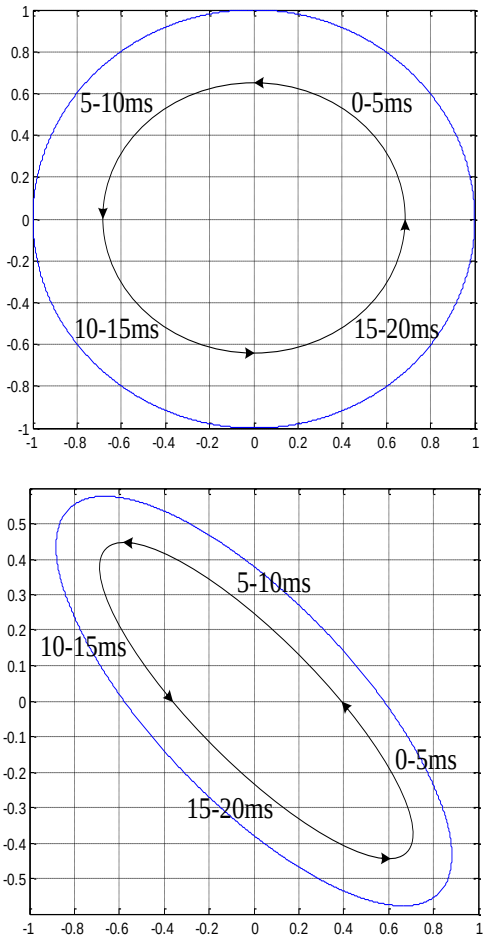

Fig. 2. Current trajectories (blue traces) in the active plane in the symmetrical (x_2-y_2) and asymmetrical (x_1-y_1) nine-phase machine during the charging mode (values are normalised with I).

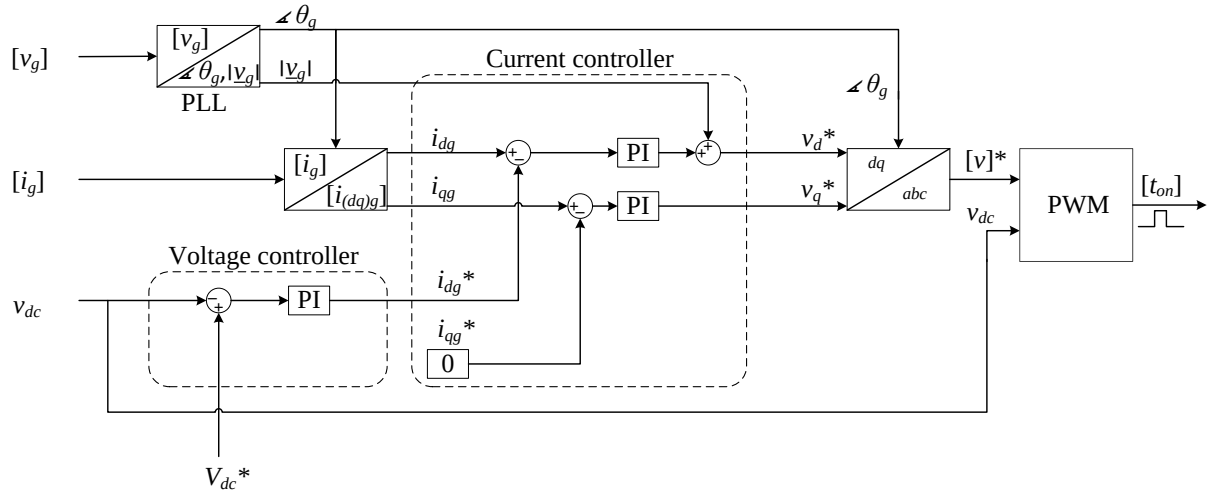

Fig. 4. Control algorithm for the charging mode.

transition from propulsion to charging mode takes place. The software for the control of the inverter/rectifier will however change, as described in the next Section.

IV. Control Algorithm for the Proposed Configurations

The theoretical results of Sections II and III imply that sets of three three-phase windings of nine-phase machines in selected configurations will behave as simple resistance-inductance passive components during the charging process. In essence, the impedances presented to the current flow will be composed of stator leakage inductance and stator resistance [19]. The simplified equivalent circuit model of the system for the charging mode is presented in Fig. 3. Thus, the configuration can be controlled like a standard three-phase voltage source rectifier.

Common way of controlling the configuration from Fig. 3 is voltage oriented control (VOC), which is shown in Fig. 4. For clarity, decoupling network at the output of the current controllers, which is required for a proper control, is not shown in Fig. 4. Control algorithm requires measurements of grid voltages, grid currents, and the dc-bus voltage.

VOC requires the information on the grid voltage position. A phase locked loop (PLL) block is widely employed for these purposes. This information is then used to transform grid currents into the grid voltage oriented rotating (*d*-*q*) reference frame. Keeping the *q*-axis current component at zero at all times insures unity power operation, and *d*-axis component can be used for achieving a desired charging power.

From Fig. 4 it can be seen that reference currents are subtracted from measured currents, unlike in the standard drive current controllers. The reason for this is that when the amplitude of inverter voltages increases, voltage on the filter (i.e. charging current) decreases, and vice versa. Thus, when the charging current increases, inverter output voltage has to decrease.

The *q*-axis component of the reference current is equal to zero. The *d*-axis component can be obtained in two ways, which correspond to two charging modes demanded by the

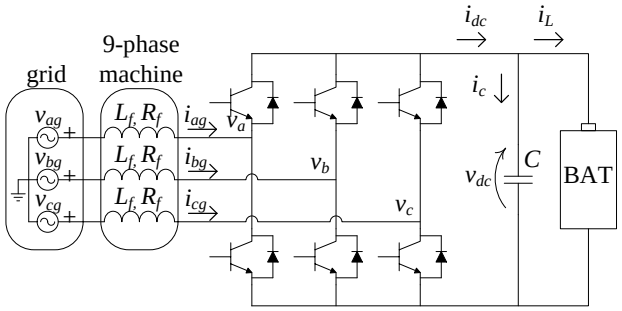

Fig. 3. Equivalent charging scheme.

battery. The CC-CV (constant current-constant voltage) mode [22] is the most common method of battery charging. In CC mode the battery is charged with a constant current, matching the maximum charging current. When voltage reaches a certain cut-off level, the charging mode switches to CV; the battery gets now charged from the constant voltage source. Charging typically stops when current drops below the value of 10% of the maximum current, and that represents the end of the charging process. Thus, in CV mode, *d*-axis component of the reference current is actually obtained from the PI dc voltage controller (Fig. 4).

The *dq* current components are not decoupled. This complicates the control due the fact that the change of either component causes change in both *d*-*q* components. For this reason, a decoupling network, which is shown in Fig. 5, is mandatory. The decoupling network adds the voltage terms $\omega_g L_f i_{qg}$ and $-\omega_g L_f i_{dg}$ to the outputs of the PI current controllers, in accordance with the mathematical model in the voltage oriented reference frame.

Before entering a PWM unit, reference signals need to be transformed from rotational to the phase reference frame. A simple carrier-based PWM with zero-sequence injection satisfies the control needs and is used in simulations.

In propulsion mode of operation nine-phase drive is operated according to the rotor field oriented control principles for nine-phase machines [23]. There is no need to control the zero-sequence components, as the case is with the

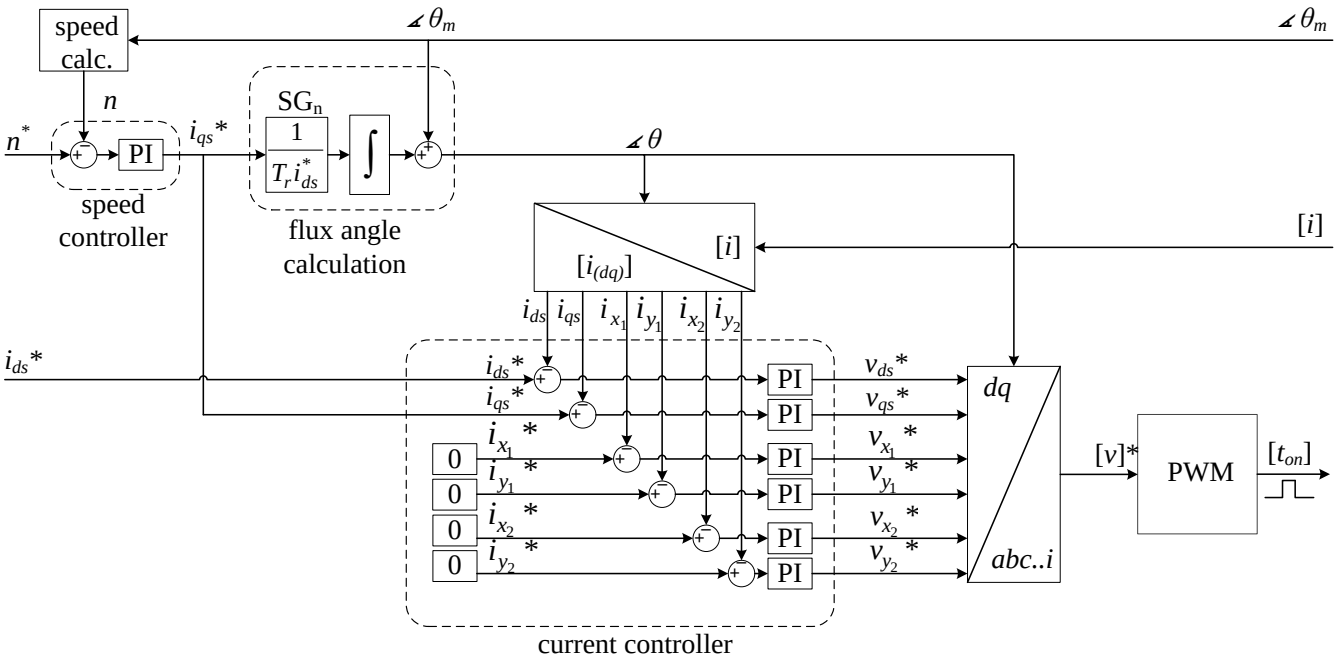

Fig. 6. Control algorithm for the propulsion mode of operation.

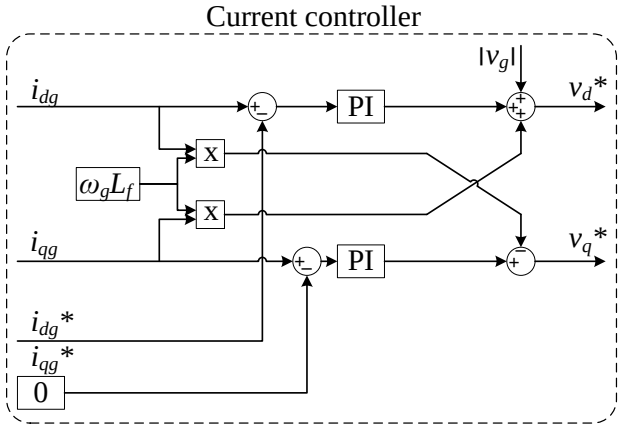

Fig. 5. Decoupling network.

configuration reported in [16]. However, three pairs of current controllers are required to ensure near-sinusoidal current in the machine in propulsion mode [19]. One possible control algorithm for the propulsion mode is presented in Fig. 6, where *x-y* current components are assumed to be in the stationary reference frame and hence *x-y* PI current controllers would have to process the ac quantities. The proportional and integral parameters of the speed controller are chosen in accordance with Fig. 6 and the output is the stator current reference i_{qs}^*. This is just one of many alternatives, which is not optimal; numerous other ways of controlling the *x-y* currents are possible.

In the propulsion mode nine-phase machines have great advantage over three-phase machines in terms of fault tolerance. The drive can be operated as long as there are at least three healthy phases in the system. This presents an important asset for the so-called 'limp-home' mode, which is typically required from EVs.

V. Simulation Results

In order to verify the theoretical results from Sections II and III, simulations of charging mode of operation for both asymmetrical and symmetrical configuration are undertaken in Matlab/SymPowerSystems software package. In both simulations grid phase voltages have rms value of 240V and 50Hz frequency. Battery is represented with a single resistor R_L = 0.5 Ω and an ideal voltage source E = 595V. Dc bus capacitance is C_{dc}=1.5mF, inverter switching frequency 2kHz, and dead time 6μs. The 50 Hz nine-phase induction machine per-phase parameters are: $R_s = R_r$ = 6 Ω, $L_{ys} = L_{yr}$ = 0.09H, L_m = 0.515H, two pole pairs, J = 0.1kgm^2.

A. Symmetrical Nine-Phase Machine

Configuration with a symmetrical nine-phase machine is simulated first in the charging mode. The charging is performed only in the continuous voltage (CV) regime, in which the dc bus voltage is regulated. CC mode is not simulated due to the similarity with the CV mode, as it regulates the battery charging current by adjusting the dc bus voltage. The dc bus voltage reference value is set to 600V.

Fig. 7a shows grid phase voltage and current. Grid voltage is obtained from an ideal sinusoidal voltage source, thus it is a perfect sine wave. The grid current has a ripple caused by the pulse width modulation of the leg voltages. The amplitude of the ripple is dependent on the machine stator leakage inductance, as it performs the function of the current filter. It varies in time due to the fixed switching frequency. It can be seen from Fig. 7a that the fundamental of the grid current and phase voltage are in phase, thus the operation is with the unity power factor at the grid side.

As noted in the Section IV, the inner control loop is the grid current control. The grid current components i_{dg} and i_{qg} that are regulated are presented in Fig. 7b. The *q*-axis component

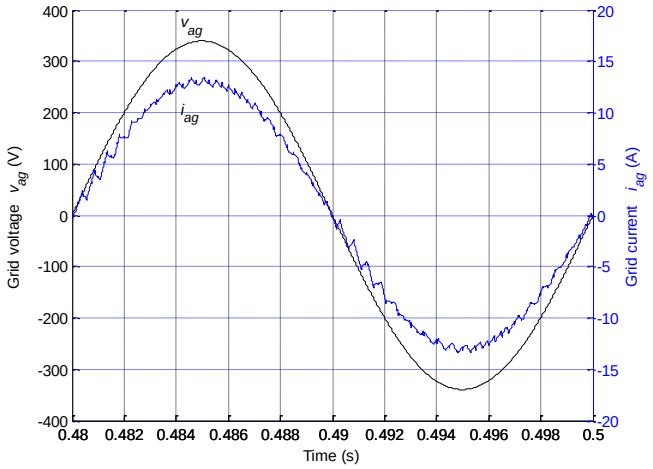

Fig. 7. Grid phase voltage v_{ag} and current i_{ag} (a) and grid current components i_{dg} and i_{qg} (b).

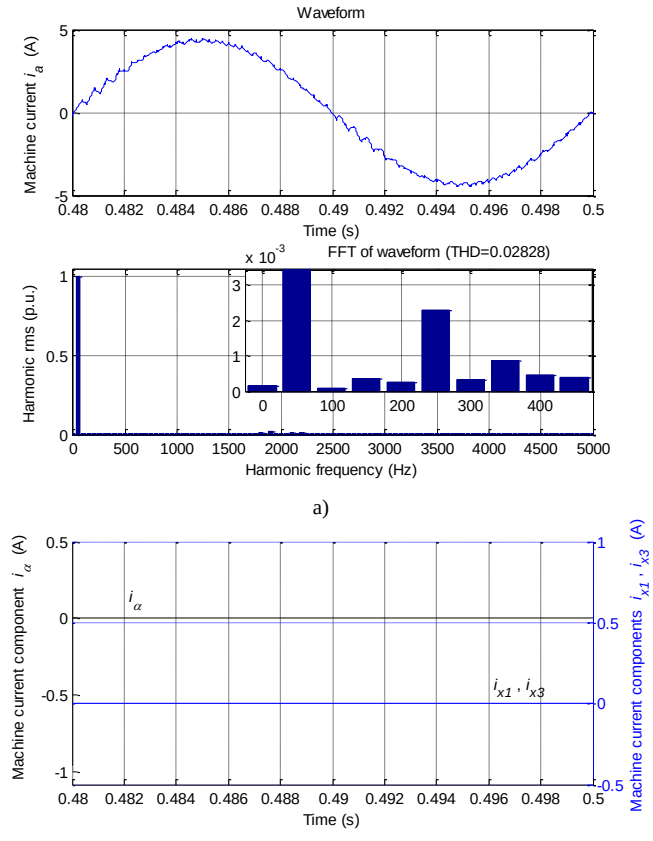

Fig. 8. Waveform and FFT of the machine phase *a* current i_a (harmonics are normalised with respect to the fundamental) (a) and machine current components in inactive planes (i_α, i_{x1}, and i_{x3}) (b).

reference is fixed to zero, and the battery is charged with the *d*-axis component. Both components follow their references. However, the current components have unequal switching ripples. This phenomenon is caused by a different effect of space vectors that are applied during PWM on the current components. Instantaneous projections of space vectors on the *d*- and *q*-axis are having higher reference tracking error in the *q*-axis than in the *d*-axis. This is due to the fact that the angle between space vectors that are applied during a switching period is low. The tracking error in the *d*-axis is proportional to its sine, while in the *q*-axis it is proportional to its cosine. This is reflected in the increased ripple of the *q*-axis current component. Since the control operates in the grid oriented reference frame and the average value of the *q*-axis current component is zero, Fig. 7b also confirms that the charging takes place at unity power factor.

The waveform and FFT of the machine phase current i_a are depicted in Fig. 8a. As can be seen, the low order harmonics are negligibly small. Mapping of all the machine phase currents into inactive planes is illustrated in Fig. 8b, where i_α, i_{x1} and i_{x3} are shown. There is obviously no excitation in any of the three planes, as predicted by (4). The only plane that is excited is the third plane, and the corresponding current component i_{x2} is presented in Fig. 9. It can be seen from the spectrum that both the switching harmonics and the small low-order harmonics, which exist in the machine phase current due to the dead time, are all mapped into this (the third) plane.

The torque developed in the machine during the charging process and the rotor speed are depicted in Fig. 10. Not only

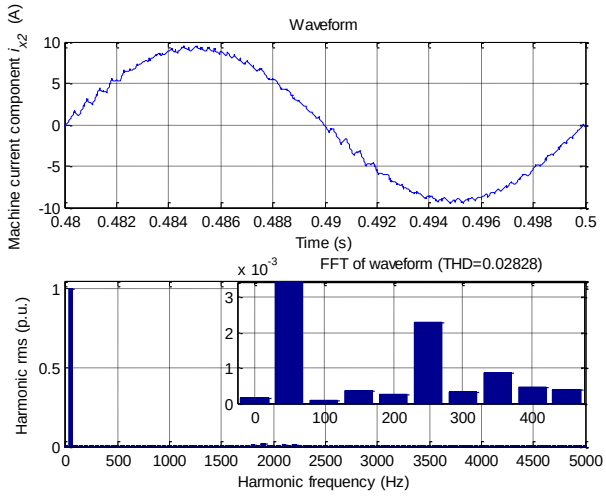

Fig. 9. Waveform and FFT of the machine current component i_{x2}.

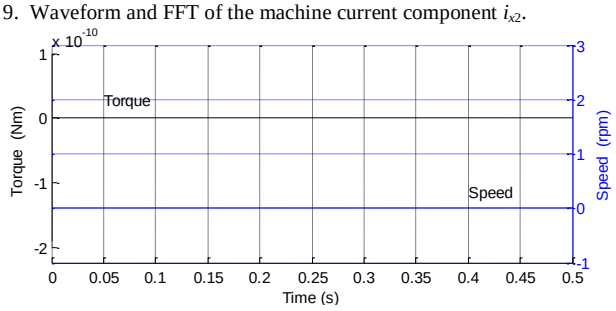

Fig. 10. Torque developed in the machine during the charging process and the rotor speed.

that the average torque is equal to zero, but the torque ripple as well remains at zero, during the whole charging period. This is caused by the field cancellation between windings of the same three-phase set. They are shifted spatially by 120 degrees and the same currents flow through them; thus they cancel each other's field and the resultant field in the machine's air gap is equal to zero, as was theoretically predicted in Section II. The speed is equal to zero during the charging process, thus the rotor stays at standstill and the machine does not have to be mechanically locked during this regime.

The converter phase voltage waveform and its spectrum are presented in Fig. 11. The 5th and the 7th harmonic, of very small values, are the consequence of the dead time of the converter. Finally, the dc bus voltage and the battery charging current are shown in Fig. 12. It can be seen that the voltage tracks its reference value, which is the outer control loop in the system. The battery charging current has the same waveform as the dc bus voltage since the battery model consists only of a resistor and an ideal voltage source.

B. Asymmetrical Nine-Phase Machine

The simulation results of the configuration with an asymmetrical nine-phase machine are presented in this sub-section. Fig. 13 shows the grid phase voltage and current and the similarity with Fig. 7a is obvious. All the other simulation results are almost identical as for the symmetrical nine-phase machine. The only, but important, difference is in the machine current components that are now as given in Fig. 14. According to (7)-(8) the non-zero current components are in the first x-y plane and along the zero-sequence axis. This is indeed the case, as is obvious from Fig. 14. There is also an asymmetrical distribution of the components in the x_1-y_1 plane (see (7)) and this is also evident in Figs. 14a and 14b. In the asymmetrical machine both the dead time harmonics and the switching harmonics map only into the second plane (i.e. x_1-y_1 plane) and the zero-sequence current.

Current components in the α-β plane and the other two x-y planes are equal to zero at all times and are hence not shown. Consequently, the torque and the speed of the machine are just the same as in Fig. 10. Thus the average torque (and the torque ripple as well) is not produced during the charging process, meaning that the asymmetrical nine-phase machine can also be integrated into the charging process, with naturally achieved zero rotor speed during the charging. All conclusions from the previous subsection are therefore valid for the asymmetrical nine-phase machine as well.

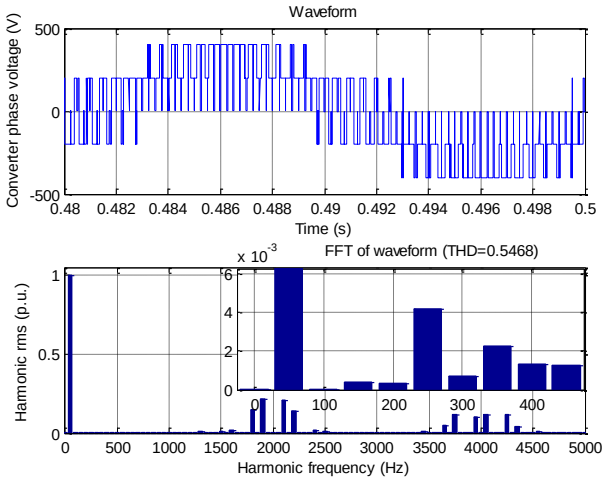

Fig. 11. Waveform and FFT of the converter's phase voltage.

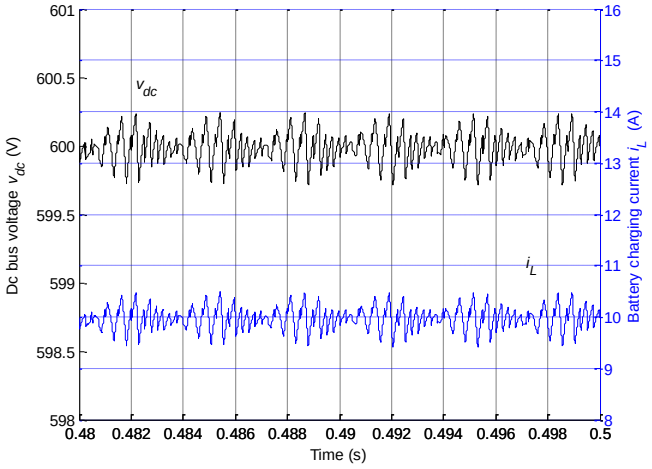

Fig. 12. Dc bus voltage v_{dc} and the battery charging current i_L.

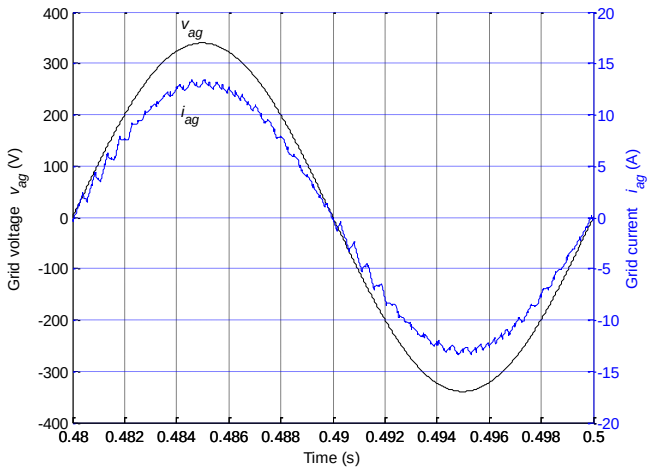

Fig. 13. Grid voltage v_{ag} and the grid current i_{ag} for an asymmetrical nine-phase machine.

VI. CONCLUSION

The paper has introduced a novel solution for fast integrated on-board charging of EVs. The two configurations, based on the application of the symmetrical and asymmetrical nine-phase machines, have advantages of unity power factor operation and zero average torque production in the machine during the charging mode. Moreover, no hardware reconfiguration is required between the propulsion and charging mode of operation. Stator leakage inductances of the machine are used to ensure filtering during charging. Theoretical viability of charging without torque production is examined, and control algorithm for the charging mode of operation is given. Theoretical results are validated by simulations.

Pre-print. Final version of this paper appears in IEEE Xplore Digital Library (http://ieeexplore.ieee.org/Xplore/guesthome.jsp).

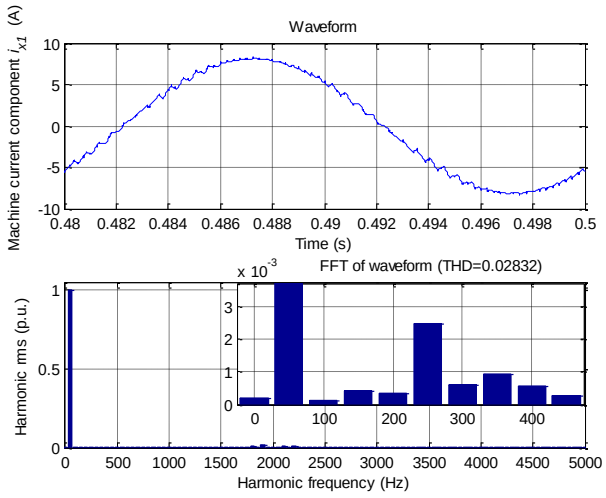

a)

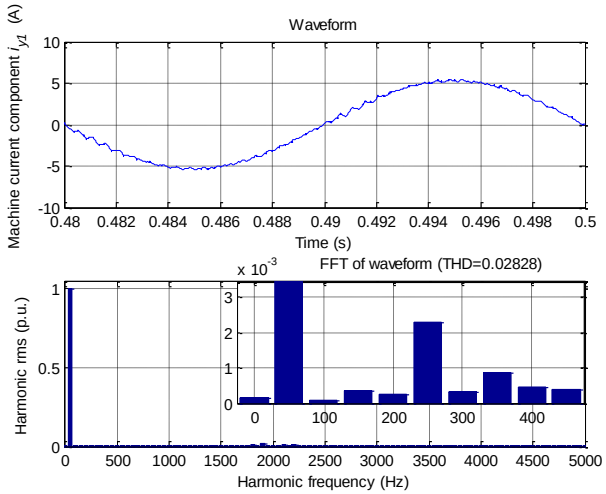

b)

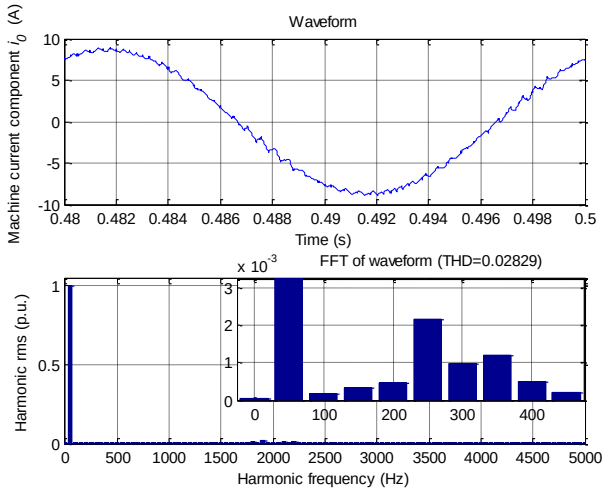

c)

Fig. 14. Waveform and FFT of the machine current components: (a) i_{x1}, (b) i_{y1}, and (c) i_0.

REFERENCES

[1] A.Y. Saber and G.K. Venayagamoorthy, "One million plug-in electric vehicles on the road by 2015", *IEEE Int. Intelligent Transportation Systems Conf. ITSC*, St. Louis, Missouri, CD-ROM, 2009.

[2] J. Harikumaran, G. Vereczki, C. Farkas, and P. Bauer, "Comparison of quick charge technologies for electric vehicle introduction in Netherlands", *IEEE Industrial Electronics Society Conf. IECON*, Montreal, Canada, pp. 2889-2895, 2012.

[3] Electromagnetic compatibility EMC, Part 3: Limits - Section 2: "Limits for harmonic current emission", IEC 1000-3-2, 1995.

[4] SAE international standards, "Power quality requirements for plug-in vehicle chargers", standard J2894/1, 2011.

[5] M. Yilmaz, and P.T. Krein, "Review of battery charger topologies, charging power levels and infrastructure for plug-in electric and hybrid vehicles", *IEEE Transactions on Power Electronics*, vol. 28, no. 5, pp. 2151 – 2169, 2013.

[6] J.R. Pillai, and B. Bak-Jensen, "Integration of vehicle-to-grid in the western Danish power system", *IEEE Transactions on Sustainable Energy*, vol. 2, no. 1, pp. 12-19, 2011.

[7] M.C. Kisacikoglu, B. Ozpineci, and L.M. Tolbert, "Examination of a PHEV bidirectional charger system for V2G reactive power compensation", *Proc. IEEE Applied Power Electronics Conf. APEC*, Palm Springs, California, pp. 458-465, 2010.

[8] "Tesla Roadster specifications", http://www.teslamotors.com/display_data/teslaroadster_specsheet.pdf, 2009.

[9] S. Haghbin, S. Lundmark, M. Alakula, and O. Carlson, "Grid-connected integrated battery chargers in vehicle applications: review and new solution", *IEEE Transactions on Industrial Electronics*, vol. 60, no. 2, pp. 459-473, 2013.

[10] J.M. Slicker, "Pulse width modulation inverter with battery charger", *US Patent* 4,491,768, 1985.

[11] M. Bertuoluzzo, N. Zabihi, and G. Buja, "Overview on battery chargers for plug-in electric vehicles", *Int. Power Electronics and Motion Control Conf. EPE-PEMC*, Novi Sad, Serbia, CD-ROM, 2012.

[12] J. De Santiago, H. Bernhoff, B. Ekergård, S. Eriksson, S. Ferhatovic, R. Waters, and M. Leijon, "Electrical motor drivelines in commercial all-electric vehicles: A review", *IEEE Transactions on Vehicular Technology*, vol. 61, no. 2, pp. 475-484, 2012.

[13] S. Kinoshita, "Electric system of electric vehicle", *US Patent* No. 5,629,603, 1997.

[14] F. Lacressonniere and B. Cassoret, "Converter used as a battery charger and a motor speed controller in an industrial truck", *Proc. European Conference on Power Electronics and Applications EPE*, Dresden, Germany, CD-ROM, 2005.

[15] S. Haghbin, S. Lundmark, M. Alakula, and O. Carlson, "An isolated high-power integrated charger in electrified-vehicle applications", *IEEE Transactions on Vehicular Technology*, vol. 60, no. 9, pp. 4115-4126, 2011.

[16] L. De Sousa, B. Silvestre, and B. Bouchez, "A combined multiphase electric drive and fast battery charger for electric vehicles", *Proc. IEEE Vehicle Power and Propulsion Conference VPPC*, Lille, France, CD-ROM, 2010.

[17] A. Sandulescu, F. Meinguet, X. Kestelyn, E. Semail, and A. Bruyere, "Flux-weakening operation of open-end winding drive integrating a cost-effective high-power charger", *IET Electrical Systems in Transportation* (to be published), 2013.

[18] E. Levi, "Multiphase electric machines for variable-speed applications", *IEEE Transactions on Industrial Electronics*, vol. 55, no. 5, pp. 1893-1909, 2008.

[19] E. Levi, R. Bojoi, F. Profumo, H.A. Toliyat, and S. Williamson, "Multiphase induction motor drives - a technology status review", *IET Electric Power Applications*, vol. 1, no. 4, pp. 489-516, 2007.

[20] A.A. Rockhill and T.A. Lipo, "A simplified model of a nine-phase synchronous machine using vector space decomposition", *Electric Power Components and Systems*, vol. 38, no. 4, pp. 477-489, 2010.

[21] M.M Wogari and O. Ojo, "Nine-phase interior permanent magnet motor for electric vehicle drive", *IEEE Power and Energy Society General Meeting*, Detroit, Michigan, CD-ROM, 2011.

[22] S. Dusmez, A. Cook, and A. Khaligh, "Comprehensive analysis of high quality power converters for level 3 off-board chargers", *Proc. IEEE Vehicle Power and Propulsion Conf. VPPC*, Chicago, Illinois, CD-ROM, 2011.

[23] E. Levi, "FOC: Field oriented control", in *The Industrial Electronics Handbook – Power Electronics and Motor Drives* (Chapter 24), edited by B.M. Willamowski and J.D. Irwin, CRC Press, 2011.